



# Influence of support on the aerobic oxidation of HMF into FDCA over preformed Pd nanoparticle based materials



Baraa Siyo<sup>a,b</sup>, Matthias Schneider<sup>a</sup>, Jörg Radnik<sup>a</sup>, Marga-Martina Pohl<sup>a</sup>, Peter Langer<sup>a,b</sup>, Norbert Steinfeldt<sup>a,\*</sup>

<sup>a</sup> Leibniz-Institut für Katalyse e.V., Albert-Einstein-Str. 29a, 18059 Rostock, Germany

<sup>b</sup> Institut für Chemie, Universität Rostock, Albert-Einstein-Str. 3a, 18059 Rostock, Germany

## ARTICLE INFO

### Article history:

Received 20 December 2013

Received in revised form 21 February 2014

Accepted 18 March 2014

Available online 25 March 2014

### Keywords:

Pd

Nanoparticles

Supported catalysts

5-Hydroxymethylfurfural

2,5-Furandicarboxylic acid

Oxidation

## ABSTRACT

Here, the preparation and evaluation of supported nanoparticle based catalytic material is reported. Polyvinylpyrrolidone (PVP) stabilized palladium nanoparticles with a mean particle size of 1.8 nm were synthesized in ethylene glycol and subsequently deposited onto different metal oxide supports ( $\text{TiO}_2$ ,  $\gamma\text{-Al}_2\text{O}_3$ ,  $\text{KF}/\text{Al}_2\text{O}_3$ , and  $\text{ZrO}_2/\text{La}_2\text{O}_3$ ). The prepared catalysts were applied to the aerobic oxidation of 5-hydroxymethylfurfural (HMF) to 2,5-furandicarboxylic acid (FDCA) in aqueous solution at atmospheric pressure ( $T = 90^\circ\text{C}$ ,  $p_{\text{O}_2} = 1$  bar) and compared regarding their catalytic performance and stability. The highest FDCA yield (>90%) was obtained for the Pd/ $\text{ZrO}_2/\text{La}_2\text{O}_3$  catalysts which additionally showed a relatively stable catalytic performance when the material was reused. Various characterization methods including XRD, TEM, XPS, and AAS were applied to obtain information about the Pd NP before and after utilization in HMF oxidation. For the Pd/ $\text{TiO}_2$  the least changes in Pd NP structure were observed after using the material in HMF oxidation. This was attributed to a stronger interaction between the Pd NP and the  $\text{TiO}_2$  support compared to other supports used in the studies.

© 2014 Elsevier B.V. All rights reserved.

## 1. Introduction

Metallic nanoparticles dispersed onto oxide supports have been used as catalysts for the synthesis of chemicals, pharmaceuticals and for energy applications [1]. Mostly, conventional salt-impregnation methods were used for catalyst preparation, where the metal particles are formed in the presence of the support. In this case metal particle size, shape and dispersion of the catalytically active compound are influenced by a large number of parameters, e.g. the support and can therefore vary strongly [2].

In the last two decades colloid chemistry based methods have been developed to synthesize differently sized metallic NP with narrow size distribution [3–6]. Deposition of the pre-formed metal nanoparticles onto carrier materials influences the adjusted particle size distribution in many cases only moderately [7–9]. Therefore, catalytic materials synthesized by colloidal deposition methods might be considered as an interesting alternative for catalyst preparation [10]. Furthermore, this method can be also used to study the effect of the support on catalytic activity and selectivity isolated from other factors of catalyst preparation [11]. The support

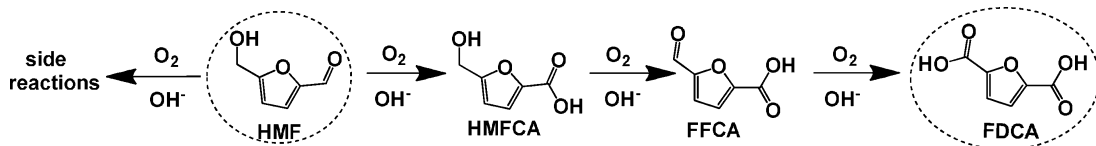
can e.g. increase the stability of the NP against coarsening, alter the structure and shape of NP, encapsulate the active NP at high temperature, transfer charge from/to the NP, supply additional reaction sites (e.g. oxygen vacancies), and stabilize intermediate reaction species [12].

5-Hydroxymethylfurfural (HMF), is considered as a platform chemical and, after its reduction or oxidation, as a potential starting material for several industrial applications [13]. It can be synthesized via acid catalyzed dehydration of carbohydrates (e.g. fructose or glucose) [14–17]. 2,5-Furandicarboxylic acid (FDCA) which can be formed by oxidation of HMF, is considered as one of the twelve most potentially useful biomass derived chemicals [18], and might be used as a renewable intermediate for polymers, fine chemicals, pharmaceuticals and agrochemicals [19]. In this reaction, 5-hydroxymethyl-furan-2-carboxylic acid (HMFC) and 5-formyl-furan-2-carboxylic acid (FFCA) are formed as intermediates (Scheme 1). The main difficulties in this reaction originate from the fact that a base has to be present in the reaction mixture, while the substrate (HMF) is unstable in alkaline aqueous solution [20].

The influence of the support on the oxidation of HMF to FDCA was investigated with Au [21,22], Pt [23,24] and ruthenium hydroxide based catalysts [25]. Pd based materials have already been successfully applied to the aerobic oxidation of alcohols to carbonyl groups, both in an organic and aqueous reaction media [26–31].

\* Corresponding author. Tel.: +49 0 381 1281 319; fax: +49 0 381 1281 51319.

E-mail address: [norbert.steinfeldt@catalysis.de](mailto:norbert.steinfeldt@catalysis.de) (N. Steinfeldt).



**Scheme 1.** Formal reaction scheme of the aerobic oxidation of HMF with molecular oxygen in water.

However, studies on supported Pd based materials for the HMF oxidation were explored merely using Pd/C as catalyst [32].

Previously, it was shown that the catalytic performance of PVP protected Pd NP in HMF oxidation depends on the particle size [33]. Small Pd NP with a mean diameter of 1.8 nm were more active and selective than larger ones. However, stabilization of these unsupported Pd NP by PVP in alkaline solution decreased during the reaction. Deposition of the Pd NP on solid surfaces can be considered as an option to obtain materials with higher catalytic stability. Here, the most active unsupported Pd NP species with a mean diameter of 1.8 nm delivering the highest yield of FDCA was chosen for the deposition on reducible ( $TiO_2$ ) and passive ( $ZrO_2/La_2O_3$ ,  $\gamma-Al_2O_3$ ,  $KF/Al_2O_3$ ) support materials. The aim of the presented work is to elucidate the role of metal oxide support on the catalytic performance and stability of Pd NP based materials in HMF oxidation. Therefore, particle size and electronic structure of the NP both after NP deposition on the respective support and after using the materials as catalyst in HMF oxidation were investigated. Additionally, the reusability of the catalysts were studied.

## 2. Experimental

### 2.1. Materials

5-Hydroxymethylfurfural (HMF) (>99%), 2,5-furandicarboxylic acid (FDCA) (>97%), polyvinylpyrrolidone K30 (PVP), sodium tetrachloropalladate  $Na_2PdCl_4$  (>98%) were purchased from Sigma-Aldrich, while 5-hydroxymethyl-furan-2-carboxylic acid (HMFCA) was obtained from Santa-Cruz Biotechnology. 5-Formyl-furan-2-carboxylic acid (FFCA) was purchased from endothermic life science molecules, and oxygen was obtained from air-liquide. As supports  $PtO_2$  (Evonik,),  $Al_2O_3$  (Alfa-Aesar,),  $KF/Al_2O_3$  (Sigma-Aldrich) and  $ZrO_2/La_2O_3$  (MEL, 7 wt%  $La_2O_3$ ) were used. All chemicals were used as received.

### 2.2. Synthesis of Pd NP

Pd NP were synthesized in a round bottom flask equipped with a reflux-condenser with argon bubbling through the reaction mixture. Sodium tetrachloropalladate ( $Na_2PdCl_4$ ) (0.236 g, 0.80 mmol) and polyvinylpyrrolidone (0.266 g, 2.3 mmol, PVP monomer unit = 111.4 g/mol) were dissolved in 33.6 mL of ethylene glycol at room temperature. The solution was heated up to 90 °C. At this point, 6.4 mL of NaOH dissolved in ethylene glycol (0.5 M) were added dropwise to the Pd salt containing solution. The final concentration of NaOH in the synthesis solution was 80 mM. The stirred reaction mixture was kept constant at 90 °C under argon atmospheres for 3 h. Finally, the obtained black solution was cooled and stored at ambient temperature.

### 2.3. Deposition of Pd NP

2.3 mL of the Pd NP containing synthesis solution was washed with 10 mL acetone. The precipitate, separated from the liquid phase by centrifugation (3500 rpm for 10 min), was re-dissolved in 10 mL ethanol or water and added to a support/solvent suspension (0.995 g of support in 25 mL solvent) by means of a syringe pump at

25 °C over 1 h. Depending on the respective support, different times passed until the solution became clear. Finally, the solid material was separated from the solvent by centrifugation (3500 rpm, for 20 min) and dried in a dry box at 40 °C.

### 2.4. Oxidation of HMF

HMF oxidation was carried out in a 25 mL three-necked flask equipped with a reflux condenser at 90 °C. The reactor was charged with 0.4 mmol of HMF in 20 mL of water. The molar ratio of HMF to Pd was 100:1. The reactor was then placed in a preheated oil bath (100 °C). After few seconds oxygen and aqueous NaOH (0.5 M) were introduced through a septum. The oxygen flow rate was controlled by a mass flow controller (Bronkhorst) and aqueous solution of NaOH (0.5 M) was continuously added to the reaction mixture using a Hamilton syringe pump. To follow the course of the reaction, samples of 50  $\mu$ L were taken from the reaction mixture in regular time intervals using a 100  $\mu$ L Hamilton syringe. The samples were diluted with a 0.2% aqueous solution of  $H_3PO_4$  (total volume of 10 mL). Then, the samples were centrifuged to remove solids and subjected to HPLC analysis. Concentrations of observed products were obtained from calibration curves formed by injecting solutions with known concentration.

HPLC analysis: Merck-Hitachi with L-4500 diode array detector, column: Rezex ROA-Organic Acid H+ (8%) 300 × 7.8 mm (phenomenex), injection: 5  $\mu$ L, mobile phase: 0.2%  $H_3PO_4$ /water, temperature: 25 °C, flow rate: 0.8 mL/min.

### 2.5. Characterization methods

The amount of Pd on the different supports was determined by atom absorption spectroscopy (AAS) using a Perkin Elmer AAS-A Analyst 300 after pulping the solid using sulphuric acid and potassium bisulfate. In order to determine the Pd amount in the solution, 10 mL of the post reaction mixture were mixed with 10 mL aqua regia before being analyzed by AAS.

Nitrogen adsorption-desorption isotherms were collected on a BELSORP-mini II (BEL Japan, Inc.). Specific surface areas and pore size distributions were calculated from the adsorption and desorption branches of the isotherm, respectively, applying the Brunauer, Emmet and Teller (BET) equation for  $N_2$ .

The phase composition of the catalyst was determined by XRD using a theta/theta diffractometer (X'Pert Pro from Panalytical, Almelo, Netherlands) with  $Cu K\alpha$  radiation ( $\lambda = 0.15418$  nm, 40 kV, 40 mA) and a X'Celerator RTMS detector.

Transmission electron microscopy (TEM) and scanning transmission electron microscopy (STEM) images of Pd based materials were obtained at 200 kV with a JEM-ARM200F (JEOL Ltd) which is aberration-corrected by a CESCOR (CEOS). High-angle annular dark field (HAADF) imaging was operated with a spot size of 6c (approximately 0.13 nm) and a 40  $\mu$ m condenser aperture. The samples were deposited on holey carbon supported Cu-grids (mesh 300) and transferred to the microscope.

The oxidation states and the surface compositions were determined by X-ray photoelectron spectroscopy (XPS). The measurements were performed with an ESCALAB 220iXL (ThermoFisher Scientific) with monochromatic  $Al K\alpha$  radiation ( $E = 1486.6$  eV). The

**Table 1**  
Characteristics of NP deposition.

Catalyst	Solvent	Time (h)	Pd (wt%)	BET ( $\text{m}^2/\text{g}$ )	Pore volume (mL/g)	d(NP) (nm)
Pd NP			—	—		1.8 ± 0.5
Al <sub>2</sub> O <sub>3</sub>				220	0.62	
Pd/Al <sub>2</sub> O <sub>3</sub>	EtOH	24	0.45	176		2.7 ± 0.6
KF/Al <sub>2</sub> O <sub>3</sub>				25	0.06 [47]	
Pd/KF/Al <sub>2</sub> O <sub>3</sub>	EtOH	—				n.d.*
TiO <sub>2</sub>	H <sub>2</sub> O	48	0.6	101		
Pd/TiO <sub>2</sub>	EtOH	1	0.53	50	0.25 [48]	2.1 ± 0.7
	H <sub>2</sub> O	1	0.5	35		
ZrO <sub>2</sub> /La <sub>2</sub> O <sub>3</sub>				35		
Pd/ZrO <sub>2</sub> /La <sub>2</sub> O <sub>3</sub>	EtOH	—		279	0.08	
	H <sub>2</sub> O	48	0.39	252		2.6 ± 0.5

\* Not determined.

samples were fixed on a stainless steel sample holder with double adhesive carbon tape. For charge compensation a flood gun was used, the spectra were referenced to the C1s peak at 284.8 eV. The error range for the determination of the electron binding energy is estimated to be ±0.2 eV. After background subtraction the peaks were fitted with Gaussian–Lorentzian curves to determine the positions and the areas of the peaks. The surface composition was calculated from the peak areas divided by the element-specific Scofield factor and the transmission function of the spectrometer.

### 3. Results and discussion

#### 3.1. Deposition of pre-formed PVP stabilized Pd NP on metal oxide surfaces

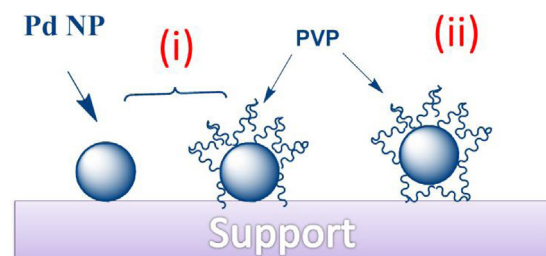
The deposition of the pre-formed PVP stabilized Pd NP on the different supports was carried out both in water and ethanol as solvent with a nominal Pd loading of 0.5 wt%. The change in the color of the PVP-Pd NP containing solvent from dark brown to approximately colorless was used as indication that most of the Pd NP were adsorbed onto the support. Depending on the respective support, different times passed until the solution became clear (see Table 1). On TiO<sub>2</sub>, Pd NP were deposited both in ethanol and water within of 1 h with the nominal loading of 0.5 wt%. The deposition of the Pd NP on KF/Al<sub>2</sub>O<sub>3</sub> and ZrO<sub>2</sub>/La<sub>2</sub>O<sub>3</sub> could only be achieved in water but after clearly longer time intervals (48 h) in comparison to titania. A faster NP deposition on TiO<sub>2</sub> compared to other supports (e.g. γ-Al<sub>2</sub>O<sub>3</sub>, ZrO<sub>2</sub>) was already observed previously for Au NP and it was shown that the NP deposition time did not depend on the point of zero charge (p.z.c.) of the particular support [11]. The same result was found here, when the deposition time was compared with the p.z.c. of the used support (p.z.c.: TiO<sub>2</sub> = 6–7 [34]; ZrO<sub>2</sub>/La<sub>2</sub>O<sub>3</sub> ~ 7 (derived from measurement of the zeta potential); γ-Al<sub>2</sub>O<sub>3</sub> = 8–9 [34]). As reason for the independence of the Au NP adsorption time from the p.z.c., the negative charge of the protecting agent (polyvinylalcohol) was suggested [11].

Table 1 summarizes BET surface and pore volume of the different supports and BET surfaces of the support after Pd loading. As expected, BET surface of the Pd/support material was moderately lower compared to the unloaded support since Pd loading was relatively low [25]. The increase in BET surface for the Pd/KF/Al<sub>2</sub>O<sub>3</sub> support is attributed to the loss of KF from the alumina surface which increases the accessibility of the pores for nitrogen (see Section 3.3). The mean pore size of TiO<sub>2</sub>, ZrO<sub>2</sub>/La<sub>2</sub>O<sub>3</sub>, and γ-Al<sub>2</sub>O<sub>3</sub> was 17.5 nm, 18 nm, and 7 nm, respectively. The obtained results indicate no correlation of BET surface, pore volume, and pore diameter with the deposition time. Because of the small pore volume (ZrO<sub>2</sub>/La<sub>2</sub>O<sub>3</sub>, TiO<sub>2</sub>) and the low pore diameter (γ-Al<sub>2</sub>O<sub>3</sub>) it is believed that the deposited Pd NP were located mainly on the external surface of the support.

The particle size distribution of Pd NP in ethylene glycol solution and on the different supports was determined using HRTEM and STEM-HAADF for unsupported NP and supported materials, respectively (see Fig. 5 and Figs. S1 and S2 in Supplementary materials). Differences in mean size between Pd NP in ethylene glycol solution and on support surface were slightly larger for Al<sub>2</sub>O<sub>3</sub> and ZrO<sub>2</sub>/La<sub>2</sub>O<sub>3</sub> compared to TiO<sub>2</sub> (see Table 1). The small increase in particle size after deposition is consistent with previous reports, which suggest that the size of pre-formed NP increases only moderately during deposition [35].

Since deposition was carried out with PVP stabilized NP, Pd NP can adsorb on the respective support with and without direct metal support interaction as shown in Fig. 1. To get an indication which of these Pd species might dominate on the single support, the supports were treated with pure PVP (15.33 mg PVP in 10 mL water corresponding to 2.3 mL PVP in NP synthesis solution) in water for 1 h (the same procedure used as for NP deposition but without metal). The amount of PVP adsorbed on catalyst surface was determined from the difference of carbon content in the water phase before and after support addition. On alumina, about 50% of the available PVP amount was adsorbed after 1 h, on titania only 7%. Using ZrO<sub>2</sub>/La<sub>2</sub>O<sub>3</sub> as support, no PVP adsorption was detected after 1 h. This finding indicates that on titania most of the deposited Pd NP should be in direct interaction with the support (species i) since in this case the Pd NP were completely adsorbed on the support after 1 h. In contrast, on alumina more Pd NP should be embedded in adsorbed PVP (species ii) compared to TiO<sub>2</sub> because of the better adsorption of PVP on the alumina surface.

A better adsorption of Au NP on TiO<sub>2</sub> compared to that on ZrO<sub>2</sub> was previously reported for 2 nm negatively polarized Au NP at pH < IEP (IEP—isoelectric point). This was explained by a higher number of positively charged hydroxyl surface groups on titania. Here, it was assumed that the adsorbed layer of ligands necessary for stabilization of the Au NP in solution was destroyed during the adsorption process. Furthermore, it was suggested that besides electrostatic interactions additional factors (e.g. van der



**Fig. 1.** Formal scheme of Pd NP species which could be formed during NP deposition on the support surface.

**Table 2**

Catalytic results of HMF oxidation (X—HMF conversion, Y—product yield) on different supports and Pd/support materials with continuous addition of a homogeneous base (aq. NaOH).

Entry	Catalyst	X (HMF) (%)	Y (HMFCA) (%)	Y (FFCA) (%)	Y (FDCA) (%)	C-Balance
1	Without Pd	>99 (5 h)	3	0	0	0.03
2	Na <sub>2</sub> PdCl <sub>4</sub>	>99 (5 h)	10	0	3	0.13
3	ZrO <sub>2</sub> /La <sub>2</sub> O <sub>3</sub>	>99 (5 h)	5	<1	<1	0.07
4	Al <sub>2</sub> O <sub>3</sub>	>99 (6 h)	5	<1	0	0.06
5	TiO <sub>2</sub>	>99 (5 h)	4	1	<1	0.06
6	Pd-NP*	>99 (5 h)	8	0	90	0.98
7	Pd/ZrO <sub>2</sub> /La <sub>2</sub> O <sub>3</sub>	>99	7	0	90	0.97
8	Pd/KF/Al <sub>2</sub> O <sub>3</sub>	>99	7	0	91	0.98
9	Pd/Al <sub>2</sub> O <sub>3</sub>	>99	9	3	78	0.90
10	Pd/TiO <sub>2</sub> *(EtOH)	>99	19	2	62	0.83
11	Pd/TiO <sub>2</sub> (H <sub>2</sub> O)	>99	32	2	52	0.86

Reaction conditions: HMF (0.4 mmol), H<sub>2</sub>O (20 mL), molar ratio HMF/Pd = 100, O<sub>2</sub> flow rate = 35 mL/min, 363 K, aq. NaOH addition (0.5 mmol/h, 4 h), reaction time 8 h (\*7 h).

Waals interactions) might also play a role in the NP adsorption processes [9].

### 3.2. HMF oxidation

#### 3.2.1. Influence of the support

Previous studies have shown that the presence of high amounts of base in the reaction mixture foster the formation of byproducts through side reactions of HMF [32]. In order to ascertain the extent of these side reactions, a HMF oxidation experiment with addition of base and oxygen but without catalyst was monitored by HPLC. Under these conditions, the HMF was completely converted after 5 h, but only a very small amount of HMFCA could be detected (Table 2, entry 1). It was reported that at absence of catalyst in basic solution finally humins type products were formed by reactions of HMF degradation compounds such as formic acid, levulinic acid, and furan [36]. These products (levulinic acid and formic acid) were also observed by Pasini et al. [37]. FDCA was also not formed when the Pd precursor was used as catalyst (entry 2). This suggests that Pd<sup>2+</sup> ions are not able to catalyze the reaction of HMF with oxygen to the desired products. Similar results were obtained for the unloaded supports (entries 3–5). In all cases a strongly colored reaction mixture was obtained. In contrast to that, the solution was only slightly yellow colored in experiments with high FDCA yield. The strong coloring might indicate degradation of HMF in the reaction solution [24]. In the presence of Pd NP and Pd NP/support materials, the formation of byproducts decreases (entries 6–11) leading to higher molar carbon mass balances between 83 and 98% (combined yield of HMFCA, FFCA, and FDCA). Unsupported Pd NP afforded 90% yield of FDCA after 7 h at full conversion of HMF (entry 6). Pd/KF/Al<sub>2</sub>O<sub>3</sub> and Pd/ZrO<sub>2</sub>/La<sub>2</sub>O<sub>3</sub> also gave FDCA yields higher than 90% (entries 7 and 8). Utilization of Pd NP deposited on Al<sub>2</sub>O<sub>3</sub> or TiO<sub>2</sub> (entries 9 and 10) led to lower FDCA yields of 78% and 62%, respectively, and lower mass balances. The influence of the support on FDCA yield is further demonstrated when comparing results for TiO<sub>2</sub> in Table 2 (entries 10 and 11). Also the yields of HMFCA varied between 1 and 32% depending on the catalyst material.

The temporal evolution of HMF conversion and product yield using the different materials are compared in Fig. 2. Generally, differences in HMF conversion are very small and HMF was fully consumed after 1.5 h (NaOH/HMF ratio = 1.8). The highest concentration of the intermediate HMFCA was always found at slightly earlier times than in the case of FFCA (Fig. 2b and c). TiO<sub>2</sub> supported Pd NP showed the highest HMFCA yield. However, while FFCA was completely oxidized to FDCA, HMFCA oxidation stopped after 2 h. During this time interval also most of FDCA was formed. As no additional HMFCA was formed at this time ( $X(\text{HMF}) = 1$ ), it can be assumed that active Pd surface sites lost their capability to oxidize HMFCA after 2 h. This might be due to the partial blocking of active Pd surface sites by adsorbed organic molecules which are formed

during the oxidation as recently observed for HMF oxidation with Au/CeO<sub>2</sub> and Au/TiO<sub>2</sub> catalysts [21].

Interestingly, in contrast to HMFCA transformation, oxidation of FFCA proceeded until it was completely converted. In order to exclude that FFCA might be converted to FDCA without participation of Pd NP, an experiment was performed under identical conditions (35 mL/min O<sub>2</sub>, 1 mL/h NaOH (0.5 M, 4 h) and 90 °C) using FFCA (0.15 mmol) as substrate in the absence of the solid catalyst. Here, only a very slow amount of FFCA was converted (12% conversion of FFCA in 6 h) and FDCA was not formed. These findings strongly suggest that the supported Pd NP catalyze the transformation of FFCA to FDCA even when oxidation of HMFCA was already diminished. The results suggest that the oxidation of HMFCA to FFCA and that of FFCA to FDCA could occur on different Pd surface sites. It is worth noting, that this behavior was already observed using unsupported Pd NP [33].

The stability of FDCA was studied under identical reaction conditions. In this case FDCA (0.4 mmol) was used instead of HMF as reactant in the presence of Pd/ZrO<sub>2</sub>/La<sub>2</sub>O<sub>3</sub>, Pd/TiO<sub>2</sub>, or Pd/Al<sub>2</sub>O<sub>3</sub>. The FDCA concentration remained unchanged after a time interval of 5 h. Thus, FDCA degradation did not seem to occur to a measurable extent under these conditions as recently observed with Au/TiO<sub>2</sub> catalyst [21].

To study the influence of leached Pd on HMF oxidation, the process was stopped after 1 h, the catalyst (Pd/TiO<sub>2</sub>, Pd/ZrO<sub>2</sub>/La<sub>2</sub>O<sub>3</sub>) was separated from reaction mixture and the remaining solution was further reacted up to 8 h. The results showed that after catalyst removal the amount of HMFCA, FFCA and FDCA remained unchanged (Fig. S3a and b in SM). These results indicate that either no Pd NP leached from the catalyst or that those leached Pd NP were not catalytically active anymore. Analysis of the final reaction mixture revealed that after 8 h about 3% Pd had leached from the Pd/TiO<sub>2</sub> catalyst into the solution. In case of Pd/ZrO<sub>2</sub>/La<sub>2</sub>O<sub>3</sub> about 6% leached Pd were found. This solution, which contained higher amount of leached Pd than in former experiments, was further reacted for 8 h after catalyst separation. Additionally, HMFCA (0.08 mmol) and FFCA (0.156 mmol) were added to this solution to investigate whether the leached Pd can oxidize the intermediates. Also in this case the concentration of both intermediates FFCA and HMFCA remained unchanged (Fig. S4 in SM). The results obtained indicate that the HMF transformation was catalyzed by the Pd/support materials and not by leached Pd.

HMF oxidation on these materials was also conducted without addition of homogeneous base (Table 3). Without base, HMF conversion on the Pd based materials was slow and FDCA was formed only in trace amounts.

#### 3.2.2. Influence of rate of base addition

Since the Pd/ZrO<sub>2</sub>/La<sub>2</sub>O<sub>3</sub> catalyst gave the highest FDCA yields, this catalyst was chosen to study the effect of the rate of base

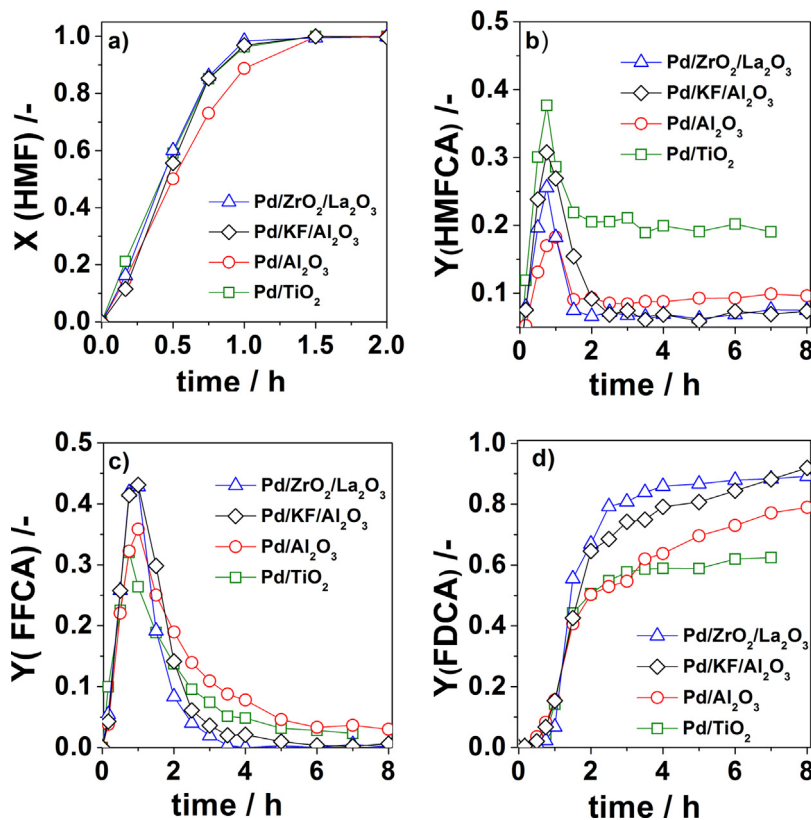


**Fig. 2.** Plots of HMF conversion (a) and product yields (b–d) versus time on Pd/support catalysts (reaction conditions: HMF (0.4 mmol), H<sub>2</sub>O (20 mL), HMF/Pd = 100 (mol/mol), O<sub>2</sub> flow rate (35 mL/min), 363 K, aq. NaOH addition [0.5 mmol/h, 4 h]).

addition on the HMF conversion and product formation over time. In these experiments, the aqueous NaOH solution (0.5 M) was continuously added to the reaction mixture with different flow rates (0.5, 1 and 2 mL/h). Base is believed to deprotonate the alcohol side chain to form an alkoxy intermediate [38] and to increase the solubility of FDCA which is low in base free solution. Hence, precipitation of the formed FDCA onto the catalyst surface may hamper the reaction [39].

The conversion and yield versus time plots (Fig. 3) show that the rate of all steps in HMF oxidation depends strongly on base concentration in the reaction mixture and the rates of formation and conversion of all investigated intermediates increased with faster base addition. At the highest flow rate (2 mL/h), the intermediates HMFCA and FFCA were almost completely transformed after 1 h (NaOH/HMF ratio = 2.5) and a FDCA yield of 80% was obtained. Constant values of carbon mass balance (0.82) after 0.5 h reaction time ( $X(\text{HMF})=1$ ) suggest that the formation of byproducts occurred at the early stage of the reaction (<0.5 h). The highest FDCA yield (90%) was obtained when the base was added with at a rate of 1 mL/h. In contrast to Au based materials FDCA can be obtained in high yields on Pd already at relatively low NaOH/HMF ratios (<2.5) [32]. At the slowest NaOH addition rate (0.5 mL/h), HMF conversion was completely after 2 h and FDCA was formed in 70% yield after 8 h. The influence of the nature of base on HMF oxidation was studied recently in presence of

Pt/C catalyst by Rass et al. They observed heavy HMF degradation from the beginning of the reaction using a NaOH/HMF ratio of 4 [24]. When the reaction was carried out under moderately basic conditions (using NaHCO<sub>3</sub> instead of NaOH) higher yields of FDCA were obtained and byproduct formation was suppressed.

The rate of base addition also has an influence on the amount of Pd leached from the support. When 4 mL of 0.5 M aq. NaOH were immediately added to the Pd/Al<sub>2</sub>O<sub>3</sub> or Pd/ZrO<sub>2</sub>/La<sub>2</sub>O<sub>3</sub> catalyst suspended in pure water (20 mL, 90 °C), the Pd/Al<sub>2</sub>O<sub>3</sub> lost about 17% and the Pd/ZrO<sub>2</sub>/La<sub>2</sub>O<sub>3</sub> catalyst about 12% of its available Pd amount after 8 h. In contrast, if the base was added continuously with different rate base addition of aq. NaOH (0.5 M) 2, 1, and 0.5 mL/h to the reaction mixture over 2, 4 and 8 h, respectively. Under these conditions, the loss of Pd from the Pd/ZrO<sub>2</sub>/La<sub>2</sub>O<sub>3</sub> catalyst amounted to 12, 6 and 2%, respectively.

### 3.2.3. Catalyst stability and reusability

In order to obtain information about the catalytic stability of the Pd based materials, the Pd/ZrO<sub>2</sub>/La<sub>2</sub>O<sub>3</sub>, Pd/KF/Al<sub>2</sub>O<sub>3</sub>, and Pd/TiO<sub>2</sub> catalysts were reused. For recycling, the solid material was separated from the reaction mixture by centrifugation, washed once with water and dried at 40 °C. Material loss due to sampling for a single run on Pd/ZrO<sub>2</sub>/La<sub>2</sub>O<sub>3</sub> and Pd/TiO<sub>2</sub> was at about 7% found by weighing of the material before and after reaction. Plots of HMF conversion and product yields versus time are shown in Figs. S5–S7

**Table 3**

Catalytic results of HMF oxidation ( $X$ —HMF conversion,  $Y$ —product yield) on different Pd NP/support catalysts without addition of homogeneous base.

Entry	Catalyst	$X(\text{HMF})$ (%)	$Y(\text{HMFCA})$ (%)	$Y(\text{FFCA})$ (%)	$Y(\text{FDCA})$ (%)	C-Balance
1	Pd/Al <sub>2</sub> O <sub>3</sub>	10	2	3	3	0.8
2	Pd/KF/Al <sub>2</sub> O <sub>3</sub>	60	30	15	3	0.8
3	Pd/ZrO <sub>2</sub> /La <sub>2</sub> O <sub>3</sub>	26	4	6	1	0.4

Reaction conditions: HMF (0.4 mmol), H<sub>2</sub>O (20 mL), molar ratio HMF/Pd = 100, O<sub>2</sub> flow rate = 35 mL/min, 363 K, aq. NaOH addition (0.5 mmol/h, 4 h), reaction time (7 h).

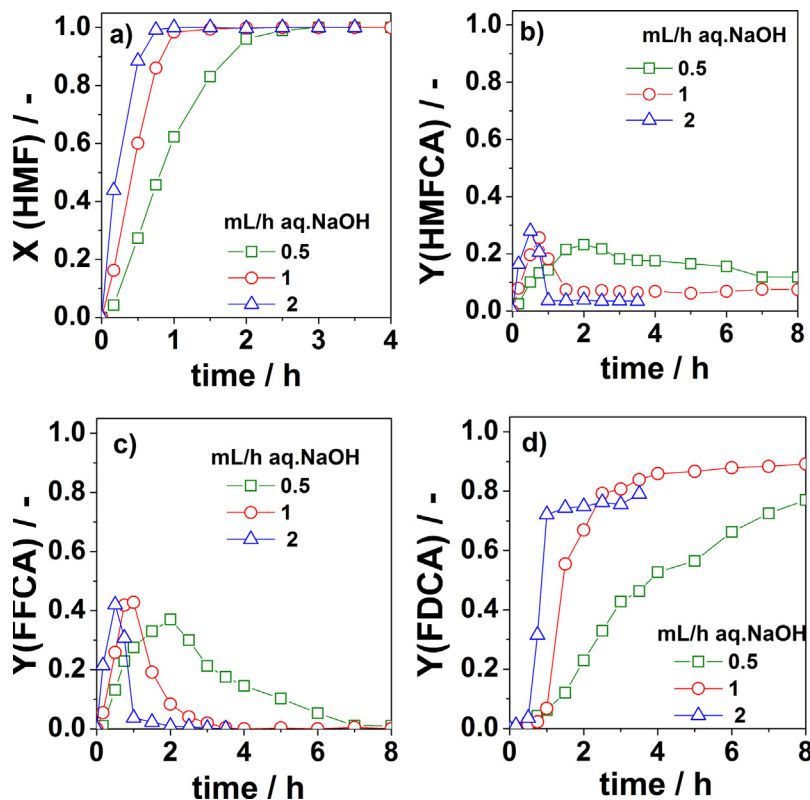


**Fig. 3.** Plots of HMF conversion (a) and product yields (b–d) versus reaction time at different rates of base addition. (conditions: HMF (0.4 mmol),  $\text{H}_2\text{O}$  (20 mL), HMF/Pd=100 (mol/mol),  $\text{O}_2$  flow rate=35 mL/min, 363 K, aq. NaOH (0.5 M), final NaOH/HMF ratio = 5).

of SM. In all runs, the HMF was completely converted after approximately 1.5 h and the formed FFCA was completely oxidized to FDCA, while oxidation of the first intermediate HMFCa did not continue after reaction times longer than 2 h. In the following experiment, the HMFCa intermediate was converted again as indicated by the concomitant yield of FDCA. The results suggest that the loss of capability to oxidize the HMFCa is a reversible effect. However, a slightly lower FDCA yield was observed in each consecutive run. Results of different runs observed after 8 h reaction time are summarized in Table 4. For the Pd/ZrO<sub>2</sub>/La<sub>2</sub>O<sub>3</sub> material the yield of FDCA decreased slightly from 90% to 86% after three runs. A lower FDCA yield was also observed for Pd/TiO<sub>2</sub> (62% → 54%). In this context it should be mentioned that Pd leaching from ZrO<sub>2</sub>/La<sub>2</sub>O<sub>3</sub> support decreased with increasing number of runs (6% in first run, 3% in third run). For the Pd/KF/Al<sub>2</sub>O<sub>3</sub> catalyst the difference in FDCA yield between the first and the second run was larger (91% → 55%). In all cases, an increase in HMFCa yield was detected with an increasing number of runs. A similar behavior, a slight decrease of the FDCA yield during recycling experiments, has previously been observed for Au/CeO<sub>2</sub> catalysts [21]. A bimetallic Au/Cu/TiO<sub>2</sub> catalyst showed more stable catalytic performances, however, the catalyst was tested under conditions leading to high yields of HMFCa compared to FDCA [37]. A stable catalytic performance was also observed for a Pt/Bi/C catalyst using NaHCO<sub>3</sub> as base [24].

**Table 4**

Results of reusability tests on Pd/support catalysts with continuous addition of homogeneous base;  $X(\text{HMF}) = 100\%$ .

Catalyst	First use			Second use			Third use		
	Y% HMFCa	Y% FFCA	Y% FDCA	Y% HMFCa	Y% FFCA	Y% FDCA	Y% HMFCa	Y% FFCA	Y% FDCA
Pd/ZrO <sub>2</sub> /La <sub>2</sub> O <sub>3</sub>	7	0	90	12	0	87	12	2	86
Pd/KF/Al <sub>2</sub> O <sub>3</sub>	7	0	91	43	0	55	—	—	—
Pd/TiO <sub>2</sub> *	19	2	62	19	2	59	26	0	54

Reaction conditions: HMF (0.4 mmol),  $\text{H}_2\text{O}$  (20 mL), HMF/Pd = 100 (mol/mol),  $\text{O}_2$  flow rate: 35 mL/min, 363 K, aq. NaOH addition (0.5 mmol/h, 4 h), reaction time: 8 h (\*7 h).

### 3.3. Characterization of fresh and used catalysts

The fresh and used catalysts were subjected to XRD to determine possible structural changes of the materials (Fig. 4). Reflections from metallic Pd NP were not observed because of the low Pd loading (0.5 wt%). Diffraction patterns of TiO<sub>2</sub>, ZrO<sub>2</sub>/La<sub>2</sub>O<sub>3</sub>, and Al<sub>2</sub>O<sub>3</sub> were neither influenced by the Pd deposition nor by HMF oxidation at 90 °C in basic solution. In case of Al<sub>2</sub>O<sub>3</sub> and ZrO<sub>2</sub>/La<sub>2</sub>O<sub>3</sub> only very broad XRD signals appeared which might be caused by a small crystallite size and/or by a high portion of amorphous phases. SEM images of the ZrO<sub>2</sub>/La<sub>2</sub>O<sub>3</sub> material, before and after application in HMF oxidation (Fig. S8, SM) imply that the morphology of the ZrO<sub>2</sub>/La<sub>2</sub>O<sub>3</sub> particles did not change during the HMF oxidation.

For Pd/KF/Al<sub>2</sub>O<sub>3</sub> (see Fig. 4d) the diffraction pattern changed both during Pd loading and during HMF oxidation but the alumina structure remained intact. The K<sub>3</sub>AlF<sub>6</sub> phase (PDF-Nr. 000-0615) observed after Pd NP deposition disappeared and a PdF<sub>4</sub> phase (PDF-Nr. 070-0717) was formed during the reaction. Additional peaks can be attributed to a K<sub>2</sub>O phase (PDF-Nr. 013-0373). The observed differences in phase compositions might be responsible for the relatively high loss of material (33%) in a single experiment as well as for the differences in the catalytic performance between first and second use (FDCA yield: 1st use—91%; 2nd use—55%).

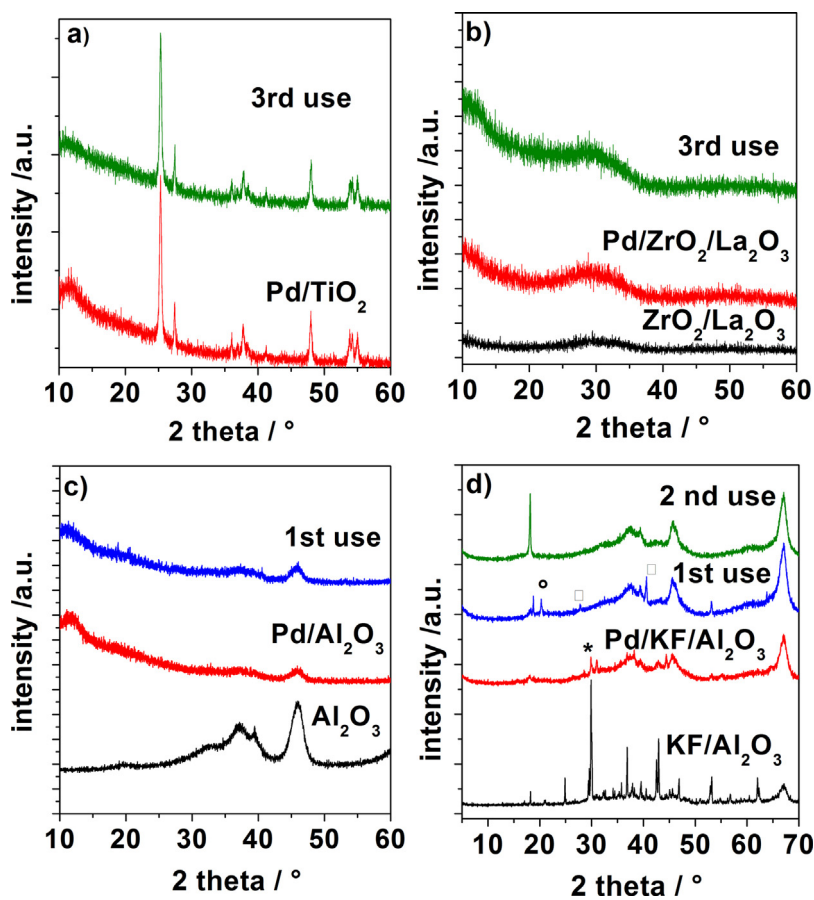


**Fig. 4.** Influence of Pd NP deposition and HMF oxidation on the XRD pattern of the Pd/support materials (a)  $\text{TiO}_2$ , (b)  $\text{ZrO}_2/\text{La}_2\text{O}_3$ , (c)  $\text{Al}_2\text{O}_3$ , and (d)  $\text{KF}/\text{Al}_2\text{O}_3$  (\*— $\text{K}_3\text{AlF}_6$ , □— $\text{K}_2\text{O}$ , ○— $\text{PdF}_4$ ).

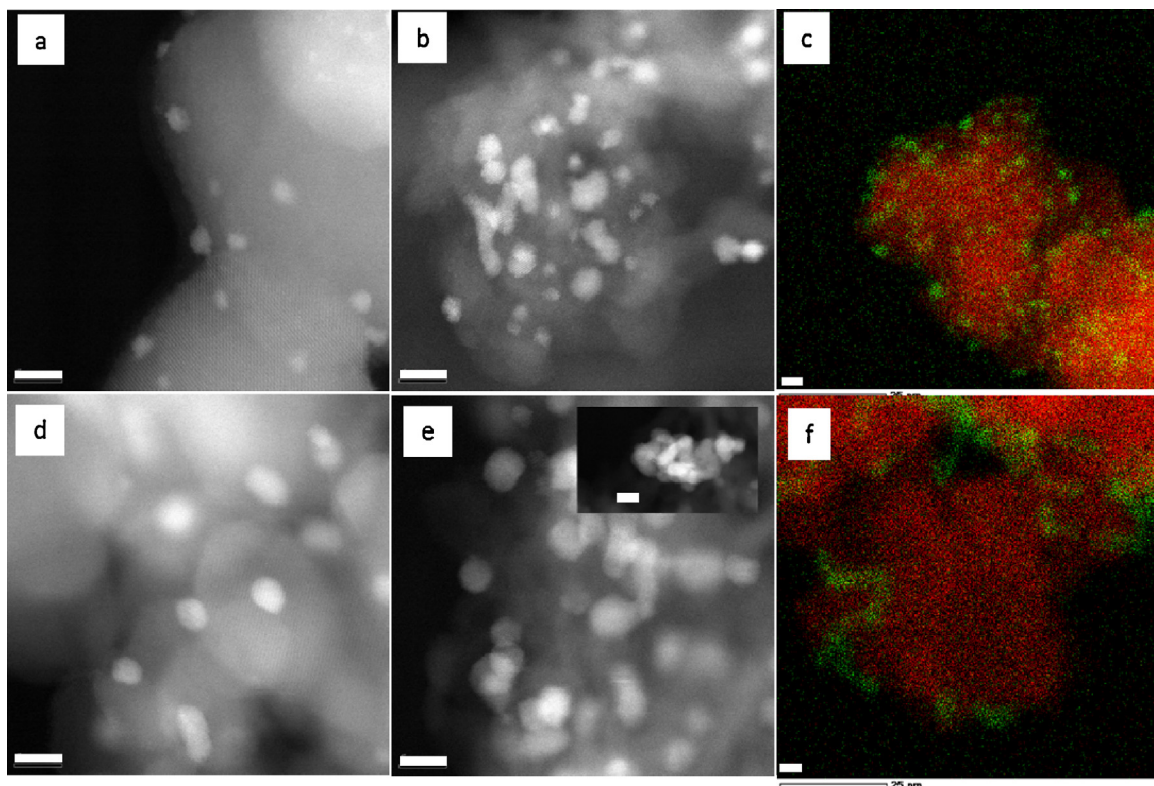


**Fig. 5.** STEM-HAADF images (a, b, d and e) and results of Pd mapping (c and f) on Pd NP supported on  $\text{TiO}_2$  (a and d),  $\text{Al}_2\text{O}_3$  (b and e), and  $\text{ZrO}_2/\text{La}_2\text{O}_3$  (c and f) after NP deposition (a–c) and after third use (d–f) in HMF oxidation ( $\text{Pd}/\text{Al}_2\text{O}_3$  after first use, insert in (b) shows structure of a large Pd aggregate; scale bar: 5 nm).

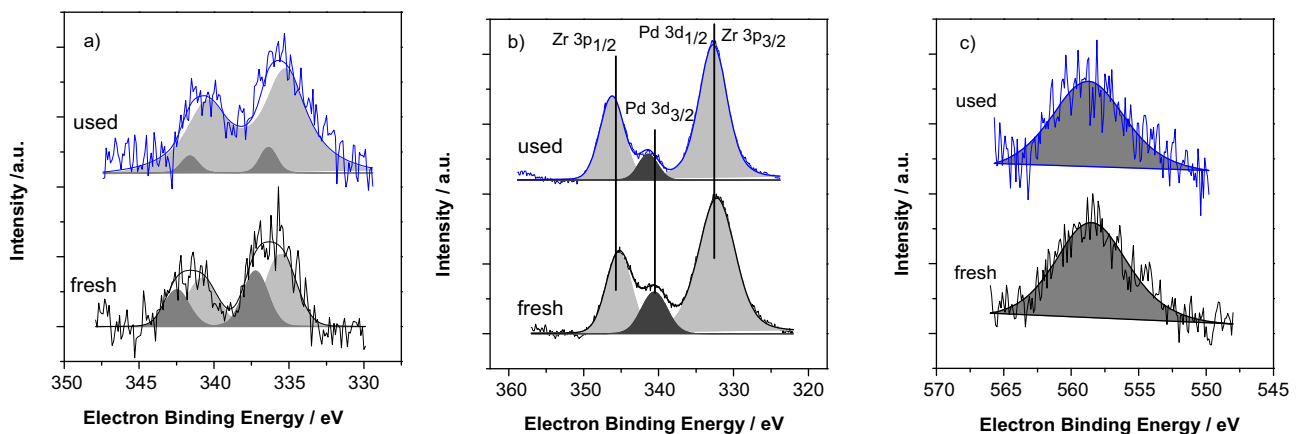


**Fig. 6.** XPS spectra of (a) the Pd3d electrons from the fresh and used (3×) Pd/TiO<sub>2</sub> catalysts, (b) the Zr3p and Pd 3d electrons and (c) the Pd3p electrons from the fresh and used (3×) Pd/ZrO<sub>2</sub>/La<sub>2</sub>O<sub>3</sub> catalysts.

It is generally accepted that the catalytic performance of NP based catalysts depends on the geometric and electronic structure of the active sites [40] and the nature of support [41,42]. The influence of HMF oxidation on Pd NP structure for the different supports was studied by TEM. Fig. 5 shows STEM-HAADF images of freshly prepared Pd/TiO<sub>2</sub>, Pd/Al<sub>2</sub>O<sub>3</sub>, and Pd/ZrO<sub>2</sub>/La<sub>2</sub>O<sub>3</sub> catalysts and after utilization in the HMF oxidation. For Pd/ZrO<sub>2</sub>/La<sub>2</sub>O<sub>3</sub> more reliable results were obtained by element mapping with EDX because the electron density of the ZrO<sub>2</sub>/La<sub>2</sub>O<sub>3</sub> support (La: atomic number 57, Zr: atomic number 40) is higher and similar compared to Pd (atomic number 46), respectively.

The utilization of the materials in HMF oxidation led to an increase in particle size, broadening of the size distribution and changing of the shape (see also Table 1 and Fig. S2, SM). The extent of the observed changes depended on the support and seems to be highest for Al<sub>2</sub>O<sub>3</sub>. Here large Pd aggregates with mean sizes larger than 20 nm were observed already after the first use (see inset Fig. 5e). On the ZrO<sub>2</sub>/La<sub>2</sub>O<sub>3</sub> support the formed Pd aggregates were smaller although the material was used three times. Furthermore, the Pd aggregates seem to be more elongated. Such elongated Pd structures were also obtained when the PVP was substituted by a molecular stabilizer by means of a phase transfer to toluene at 100 °C [43]. The lowest change in particle size and shape of Pd NP after reaction was observed on titania.

In order to obtain information about the electronic structure of the supported Pd NP, the Pd/ZrO<sub>2</sub>/La<sub>2</sub>O<sub>3</sub> and Pd/TiO<sub>2</sub> catalysts were characterized by XPS both after NP deposition and after utilization in HMF oxidation. In general, the positions of the Pd XPS signals are influenced by the valence state of Pd, e.g. the binding energy for bivalent Pd is usually higher than for metallic Pd. Moreover, the electronic interaction of Pd with the support and the size of the Pd species could lead to a shift of the binding energy [44–46]. For the ZrO<sub>2</sub>/La<sub>2</sub>O<sub>3</sub> support the interpretation of the Pd3d spectra was complicated, due to the overlap of peaks of the Pd3d and Zr3p electrons. Nevertheless, it was possible to determine the maximum of the Pd3d<sub>3/2</sub> peak (340.4 eV for the fresh sample, 341.4 eV after use). Additionally, the Pd3p<sub>1/2</sub> electrons were also recorded to obtain the Pd peak position without overlapping by other peaks. The maximum at 558.6 eV for both samples, fresh and utilized, confirm that the most part of Pd is metallic and that the electronic structure of the Pd NP is not changed by the oxidation reaction (Fig. 6b and c).

In contrast to ZrO<sub>2</sub>/La<sub>2</sub>O<sub>3</sub>, on the TiO<sub>2</sub> support, metallic Pd (Fig. 6a, grey area, 3d<sub>5/2</sub> = 335.4 eV, 5d<sub>3/2</sub> = 340.6 eV) and bivalent Pd (dark grey area, 3d<sub>5/2</sub> = 337.0 eV, 3d<sub>3/2</sub> = 342.4 eV) were detected both in fresh and used Pd/TiO<sub>2</sub> samples. After the utilization in HMF oxidation, a reduction of a part of the bivalent Pd was observed in the Pd/TiO<sub>2</sub> sample, indicated by an increase of the peak area

of metallic Pd in the XPS spectra of Pd3d electrons. Bearing in mind that identical metallic Pd NP were used for the deposition on the ZrO<sub>2</sub>/La<sub>2</sub>O<sub>3</sub> and on the TiO<sub>2</sub> the presence of bivalent Pd after adsorption of Pd NP on the TiO<sub>2</sub> support (Fig. 6) is remarkable, because on passive ZrO<sub>2</sub>/La<sub>2</sub>O<sub>3</sub> only Pd NP in metallic state were detected. This observation indicates an influence of the support on the oxidation state of the deposited NP. Strong interactions between the Pd clusters and TiO<sub>2</sub> were already observed previously [44]. An additional evidence for this strong interaction is given in Fig. 7 showing the XP spectra of Ti2p electrons of the fresh and used sample. While for the fresh sample only a Ti<sup>4+</sup> peak was detected, the XPS signal of the used sample is composed of peaks of Ti<sup>4+</sup> and Ti<sup>3+</sup>. The formation of Ti<sup>3+</sup> during HMF reaction shows clearly the interaction between the Pd NP and the TiO<sub>2</sub> support. Moreover, such interactions might be also responsible for the faster adsorption of the Pd NP on TiO<sub>2</sub> compared to the ZrO<sub>2</sub>/La<sub>2</sub>O<sub>3</sub> and Al<sub>2</sub>O<sub>3</sub> supports.

During HMF reaction the population of bivalent Pd decreased probably because the Pd NP accept electrons released during the HMF oxidation. For Pt and Au based materials it was suggested that molecular oxygen played an indirect role in HMF oxidation by accepting electrons deposited to the supported metal particles [38]. The formation of Ti<sup>3+</sup> during the reaction might be explained as follows: as shown previously (Table 2) HMF oxidation on TiO<sub>2</sub>

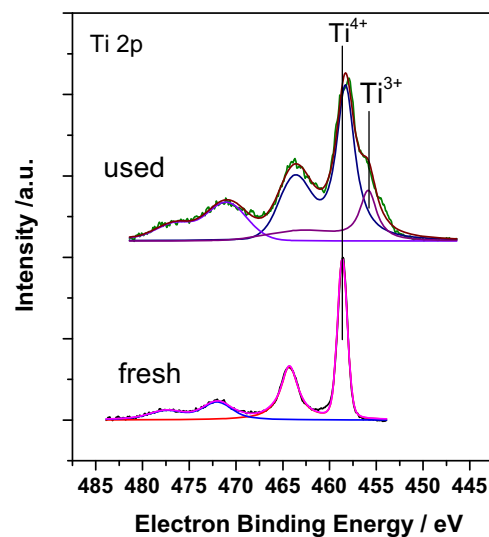


**Fig. 7.** XPS spectra of the Ti2p electrons from the fresh and used (3×) Pd/TiO<sub>2</sub> catalyst.

**Table 5**

Composition of the near-surface region of the fresh and used catalysts determined by XPS.

		Pd	N	Ti
Pd/TiO <sub>2</sub>	Fresh	0.009	0.039	1
	Used (3×)	0.008	0.014	1
Pd/ZrO <sub>2</sub> /La <sub>2</sub> O <sub>3</sub>		Pd	N	Zr
	Fresh	0.194	0.295	1
	Used (3×)	0.112	0.129	1

proceeds with byproduct formation. These byproducts might block active surface sites and make them inaccessible for molecular oxygen. Electrons which get released during the oxidation process might get transferred from the NP to the support and reduce Ti<sup>4+</sup> sites in TiO<sub>2</sub>.

During the oxidation reaction not only a low amount of Pd leached from the support but also the amount of PVP on the support surface decreased, probably by degradation, as indicated by the lower amount of nitrogen on the support surface after the reaction (see Table 5). Those NP which were formerly firmly embedded in the polymer could now migrate to either the support surface or into the liquid phase. On the support surface they could undergo, e.g. aggregation reactions, and thus form aggregated Pd structures as observed from TEM images. Because of the good adsorption of PVP on alumina (see Section 3.1), the amount of Pd NP which are embedded in adsorbed polymer (species ii in Fig. 1) should be the highest. This might be one reason that the largest aggregated Pd structures were observed on the alumina support after HMF oxidation. Differences in surface charge between the supports ZrO<sub>2</sub>/La<sub>2</sub>O<sub>3</sub> and Al<sub>2</sub>O<sub>3</sub> in basic solution are indicated by the more negative zeta potential of the respective support (pH 10: -43 mV compared to pH 10: -24 mV, measurement conditions are given in SM). This might be another reason for the lower degree of aggregation of Pd NP on ZrO<sub>2</sub>/La<sub>2</sub>O<sub>3</sub> compared to Al<sub>2</sub>O<sub>3</sub>. Degradation of PVP might also serve as explanation for comparable activities in the reusability experiments, despite the observed Pd leaching. Surface sites formerly blocked by PVP might become accessible during these processes. The low differences in FDCA yield between the successive runs in the reusability experiments might be attributed also to the formation of Pd aggregates composed of formerly smaller particles. In such structures the Pd NP would only lose a part of their surface. Hence, large parts of the former structure should still remain intact.

#### 4. Conclusions

Pd NP based materials prepared via colloidal deposition of pre-formed PVP stabilized Pd NP were used as catalysts in HMF oxidation at presence of homogeneous base. The yield of FDCA is influenced both, by the reaction conditions and by the particular support. The strength of interaction between Pd NP and the support seems to be higher for TiO<sub>2</sub> than for ZrO<sub>2</sub>/La<sub>2</sub>O<sub>3</sub> or Al<sub>2</sub>O<sub>3</sub> because of interactions between the TiO<sub>2</sub> support and the NP as evidenced from XPS. This interaction might be also responsible for the lower alteration of particle size and shape of the NP during HMF oxidation on TiO<sub>2</sub>, and for the lower Pd amount in the post reaction mixture in compared to the ZrO<sub>2</sub>/La<sub>2</sub>O<sub>3</sub> and Al<sub>2</sub>O<sub>3</sub> supports.

The highest yield of FDCA and a relatively stable catalytic performance was observed with the Pd/ZrO<sub>2</sub>/La<sub>2</sub>O<sub>3</sub> catalyst. Here, byproduct formation was generally low. In case of titania, with a stronger interaction between the Pd NP and the support, catalytic performance was also stable, but lower yields of FDCA were obtained. This might be explained by a stronger adsorption of HMF and reaction intermediates on the catalyst surface, leading to a blocking of active surface sites during the first stage of the reaction as indicated by the lower carbon mass balance. Nevertheless, this

strong interaction makes the TiO<sub>2</sub> support very interesting for further studies, e.g. by adsorption of surface modified Pd nanoparticles which could lead to a decrease of byproduct formation.

Two different processes of deactivation were observed using the Pd NP based materials: (i)—a reversible short-term deactivation by blocking of active Pd surface sites and, (ii)—an irreversible long-term deactivation by changes in Pd structure and by Pd leaching. The extent of leaching is heavily influenced by the base concentration in the reaction mixture. Particle size and shape of the NP on the support surface changed during HMF oxidation, mainly because of formerly isolated small NP aggregates. The influence of the changes in Pd structure on the catalytic performance seems to be relatively low probably because the surface of the small Pd NP in the formed aggregates remains largely intact.

#### Acknowledgments

Financial support by Tishreen University Latakia (Syria, grant number 1122/L) and the German Academic Exchange Service (DAAD) (scholarship for B.S., grant number A/09/95233) is gratefully acknowledged.

#### Appendix A. Supplementary data

Supplementary data associated with this article can be found, in the online version, at <http://dx.doi.org/10.1016/j.apcata.2014.03.020>.

#### References

- [1] R.A. Van Santen, P.W.N.M. van Leeuwen, J.A. Moulijn, B.A. Averill, *Catalysis An Integrated Approach*, Elsevier, 2000.
- [2] F. Pinna, *Catal. Today* 41 (1998) 129–137.
- [3] A. Roucoux, J. Schulz, H. Patin, *Chem. Rev.* 102 (2002) 3757–3778.
- [4] J. Park, J. Joo, S.G. Kwon, Y. Jang, T. Hyeon, *Angew. Chem. Int. Ed.* 46 (2007) 4630–4660.
- [5] T. Teranishi, M. Miyake, *Chem. Mater.* 10 (1998) 594–600.
- [6] E. Ramirez, S. Jansat, K. Philippot, P. Lecante, M. Gomez, A.M. Masdeu-Bultó, B. Chaudret, *J. Organomet. Chem.* 689 (2004) 4601–4610.
- [7] J. Schäffer, V.A. Kondratenko, N. Steinfeldt, M. Sebek, E.V. Kondratenko, *J. Catal.* 301 (2013) 210–216.
- [8] J. Croy, S. Mostafa, J. Liu, Y. Sohn, H. Heinrich, B. Cuena, *Catal. Lett.* 119 (2007) 209–216.
- [9] J.-D. Grunwaldt, C. Kiener, C. Wögerbauer, A. Baiker, *J. Catal.* 181 (1999) 223–232.
- [10] A.R. West, *Solid State Chemistry and its Applications*, Wiley, Chichester, 2014.
- [11] M. Comotti, W.-C. Li, B. Spliethoff, F. Schüth, *J. Am. Chem. Soc.* 128 (2005) 917–924.
- [12] B.R. Cuena, *Thin Solid Films* 518 (2010) 3127–3150.
- [13] A.A. Rosatella, S.P. Simeonov, R.F.M. Fraude, C.A.M. Afonso, *Green Chem.* 13 (2011) 754–793.
- [14] C. Moreau, M.N. Belgacem, A. Gandini, *Top. Catal.* 27 (2004) 11–30.
- [15] S.G. Wettstein, D.M. Alonso, E.I. Gürbüz, J.A. Dumesic, *Curr. Opin. Chem. Eng.* 1 (2012) 218–224.
- [16] C. Rasrendra, J. Soetedjo, I. Makertihartha, S. Adisasmitho, H. Heeres, *Top. Catal.* 55 (2012) 543–549.
- [17] M. Kröger, U. Prüß, K.-D. Vorlop, *Top. Catal.* 13 (2000) 237–242.
- [18] T. Werpy, G. Petersen, US Department of Energy Report, August 2004, 2004, <<http://www.osti.gov/bridge/>>.
- [19] A. Gandini, M.N. Belgacem, *Prog. Polym. Sci.* 22 (1997) 1203–1379.
- [20] S.E. Davis, M.S. Ide, R.J. Davis, *Green Chem.* 15 (2013) 17–45.
- [21] O. Casanova, S. Iborra, A. Corma, *ChemSusChem* 2 (2009) 1138–1144.
- [22] N.K. Gupta, S. Nishimura, A. Takagaki, K. Ebitani, *Green Chem.* 13 (2011) 824–827.
- [23] M. Lilga, R. Hallen, M. Gray, *Top. Catal.* 53 (2010) 1264–1269.
- [24] H.A. Rass, N. Essayem, M. Besson, *Green Chem.* 15 (2013) 2240–2251.
- [25] Y. Gorbanev, S. Kegnaes, A. Riisager, *Top. Catal.* 54 (2011) 1318–1324.
- [26] K. Mori, T. Hara, T. Mizugaki, K. Ebitani, K. Kaneda, *J. Am. Chem. Soc.* 126 (2004) 10657–10666.
- [27] M. Mifsud, K.V. Parkhomenko, I.W.C.E. Arends, R.A. Sheldon, *Tetrahedron* 66 (2010) 1040–1044.
- [28] W. Hou, N.A. Dehm, R.W. Scott, *J. Catal.* 253 (2008) 22–27.
- [29] B. Feng, Z. Hou, H. Yang, X. Wang, Y. Hu, H. Li, Y. Qiao, X. Zhao, Q. Huang, *Langmuir* 26 (2009) 2505–2513.
- [30] Z. Ma, H. Yang, Y. Qin, Y. Hao, G. Li, *J. Mol. Catal. A: Chem.* 331 (2010) 78–85.

- [31] H. Alex, N. Steinfeldt, K. Jähnisch, S. Hübner, M. Bauer, *Nanotechnol. Rev.* 3 (2014) 99–110.
- [32] S.E. Davis, L.R. Houk, E.C. Tamargo, A.K. Datye, R.J. Davis, *Catal. Today* 160 (2011) 55–60.
- [33] B. Siyo, M. Schneider, M.-M. Pohl, P. Langer, N. Steinfeldt, *Catal. Lett.* 144 (2013) 498–506.
- [34] M. Kosmulski, *J. Colloid Interface Sci.* 275 (2004) 214–224.
- [35] C. Berger-Karin, M. Sebek, M.M. Pohl, U. Bentrup, V.A. Kondratenko, N. Steinfeldt, E.V. Kondratenko, *ChemCatChem* 4 (2012) 1368–1375.
- [36] K.R. Vuyyuru, P. Strasser, *Catal. Today* 195 (2012) 144–154.
- [37] T. Pasini, M. Piccinini, M. Blosi, R. Bonelli, S. Albonetti, N. Dimitratos, J.A. Lopez-Sanchez, M. Sankar, Q. He, C.J. Kiely, G.J. Hutchings, F. Cavani, *Green Chem.* 13 (2011) 2091–2099.
- [38] S.E. Davis, B.N. Zope, R.J. Davis, *Green Chem.* 14 (2012) 143–147.
- [39] Y.Y. Gorbanev, S.K. Klitgaard, J.M. Woodley, C.H. Christensen, A. Riisager, *ChemSusChem* 2 (2009) 672–675.
- [40] H. Li, L. Li, Y. Li, *Nanotechnol. Rev.* 2 (2013) 515–528.
- [41] H.-J.F.T. Rissee, *Top. Organomet. Chem.* 16 (2005) 117–149.
- [42] A.K. Santra, D.W. Goodman, *J. Phys.: Condens. Matter* 14 (2002) 31–62.
- [43] J. Baumgard, M.-M. Pohl, U. Kragl, N. Steinfeldt, *Nanotechnol. Rev.* 3 (2014) 87–98.
- [44] W.E. Kaden, T. Wu, W.A. Kunkel, S.L. Anderson, *Science* 326 (2009) 826–829.
- [45] J.H. Kang, E.W. Shin, W.J. Kim, J.D. Park, S.H. Moon, *J. Catal.* 208 (2002) 310–320.
- [46] K. Okumura, M. Niwa, *Catal. Surv. Asia* 5 (2002) 121–126.
- [47] V. Raju, R. Radhakrishnan, S. Jaenicke, G.K. Chuab, *Catal. Today* 164 (2011) 139–142.
- [48] K.J.A. Raj, B. Viswanathan, *Indian J. Chem.* 48A (2009) 1378–1382.